

See discussions, stats, and author profiles for this publication at: <https://www.researchgate.net/publication/14568990>

# Molecular Modeling of Azole Antifungal Agents Active against *Candida albicans* . 1. A Comparative Molecular Field Analysis Study 1

ARTICLE *in* JOURNAL OF MEDICINAL CHEMISTRY · APRIL 1996

Impact Factor: 5.45 · DOI: 10.1021/jm950385+ · Source: PubMed

CITATIONS

48

READS

33

10 AUTHORS, INCLUDING:



**Jane Anastassopoulou**

National Technical University of Athens

65 PUBLICATIONS 671 CITATIONS

SEE PROFILE



**Roberta Costi**

Sapienza University of Rome

101 PUBLICATIONS 1,502 CITATIONS

SEE PROFILE



**Roberto Di Santo**

Sapienza University of Rome

129 PUBLICATIONS 1,827 CITATIONS

SEE PROFILE



**Rino Ragno**

Sapienza University of Rome

109 PUBLICATIONS 2,104 CITATIONS

SEE PROFILE

# Molecular Modeling of Azole Antifungal Agents Active against *Candida albicans*. 1. A Comparative Molecular Field Analysis Study<sup>1</sup>

Andrea Tafi,<sup>†</sup> Jane Anastassopoulou,<sup>†</sup> Theophile Theophanides,<sup>\*,†</sup> Maurizio Botta,<sup>\*,‡,§</sup> Federico Corelli,<sup>‡,§</sup> Silvio Massa,<sup>‡</sup> Marino Artico,<sup>||</sup> Roberta Costi,<sup>||</sup> Roberto Di Santo,<sup>||</sup> and Rino Ragno<sup>⊥</sup>

Chemical Engineering Department, Radiation Chemistry and Biospectroscopy Laboratory, National Technical University of Athens, Zografou Campus, 15773 Athens, Greece, Dipartimento Farmaco Chimico Tecnologico and Centro Interdipartimentale per lo Studio dei Sistemi Biomolecolari, Università degli Studi di Siena, Banchi di Sotto 55, 53100 Siena, Italy, and Dipartimento di Studi Farmaceutici and Dipartimento di Studi di Chimica e Tecnologia delle Sostanze Biologicamente Attive, Università di Roma "La Sapienza", P.le Aldo Moro 5, 00185 Roma, Italy

Received May 24, 1995<sup>®</sup>

A series of 56 azole antifungal agents belonging to chemically diverse families related to bifonazole, one of the antimycotic drugs of clinical use, were investigated using the comparative molecular field analysis (CoMFA) paradigm. The studied compounds, which have been already synthesized and reported to be active *in vitro* against *Candida albicans*, were divided into a training set and a test set. The training set consisted of 40 molecules from all the different structural classes. Due to the lack of experimental structural data on these derivatives, molecular mechanics techniques were used to obtain putative active conformations for all the compounds. The correctness of this molecular modeling work was confirmed *a posteriori* by comparison with structural data of the analog **2w** obtained by X-ray crystallographic analysis (Massa, S.; *et al.* *Eur. J. Med. Chem.* **1992**, 27, 495–502). Two different alignment rules of the training set molecules were used in this study and are based on the assumption that according to published results on azole antifungal agents, all the studied compounds exert their inhibitory activity through the coordination of their azole moiety to the protoporphyrin iron atom of the fungal lanosterol 14 $\alpha$ -demethylase enzyme. The predictive ability of each resultant CoMFA model was evaluated using a test set consisting of 16 representative compounds that belong to all the different structural classes. The best 3D-quantitative structure–activity relationship model found yields significant cross-validated, conventional, and predictive  $r^2$  values equal to 0.57, 0.95, and 0.69, respectively. The average absolute error of predictions of this model is 0.30 log units, and the structural moieties of the studied antifungal agents which are thought to contribute to the biological activity were identified. The predictive capability of this model could be exploited in further synthetic studies on antifungal azoles. Furthermore, the results obtained by using two different alignments of the inhibitors suggest that the binding mode of these molecules involves both a coordination to the iron protoporphyrin atom and an additional, likewise relevant, hydrophobic interaction with the active site.

## Introduction

Cytochromes P-450 constitute a suprafamily of enzymes which catalyze the oxidation of a large range of biological substrates. They bind dioxygen, and through a stepwise cleavage of the O<sub>2</sub> double bond incorporate one oxygen atom into nonactivated C–H bonds.<sup>2</sup> It is now widely accepted that some enzymes of the P-450 suprafamily (notably aromatase and lanosterol 14 $\alpha$ -demethylase), in extension to their role in hydroxylation and related oxygen insertion reactions, can catalyze a sequence of reactions leading to a C–C bond cleavage.<sup>3,4</sup> Cytochrome P-450-dependent lanosterol 14 $\alpha$ -demethylase (P-450<sub>DM</sub>) catalyzes the first step of the biochemically important conversion of lanosterol to cholesterol (mammals) or ergosterol (fungi) which are important constituents of the cell membrane by causing the removal of the 14 $\alpha$ -methyl group of lanosterol to give the  $\Delta^{14,15}$ -desaturated sterol.<sup>5</sup>

Under normal conditions, azole (N-substituted imidazole and triazole) antifungal antibiotics cure mycoses by inhibiting the fungal P-450<sub>DM</sub> at concentrations which are not expected to affect the corresponding host enzyme.<sup>6</sup> Azole compounds inhibit the binding of the natural substrate lanosterol to P-450<sub>DM</sub> by coordination of the ring nitrogen atom (N3 of imidazole and N4 of triazole) to the sixth coordination position of the iron atom of the enzyme protoporphyrin system.<sup>7</sup> The accumulation of 14 $\alpha$ -methylated sterols in azole-treated fungal cells affects membrane structure and functions resulting in an inhibition of the growth of fungi.<sup>6,8</sup>

Differential inhibition of this cytochrome P-450 enzyme between pathogenic fungi and man is the basis for the clinically important activity of azole antifungal agents, and the analogous differential inhibition of the enzyme between fungi and plants is also responsible for the utility of azole derivatives as agricultural antifungal agents.<sup>5,6</sup> The specificity of the inhibitors is determined by the differential complementarity between the structure of the agent and the active sites of the fungal and host enzymes.<sup>9</sup> In fact, one of the reasons to continue the search for better antifungal agents is to increase their specificity toward fungal enzymes. This is an important goal especially under pathological circum-

\* To whom correspondence should be addressed.

<sup>†</sup> Chemical Engineering Department.

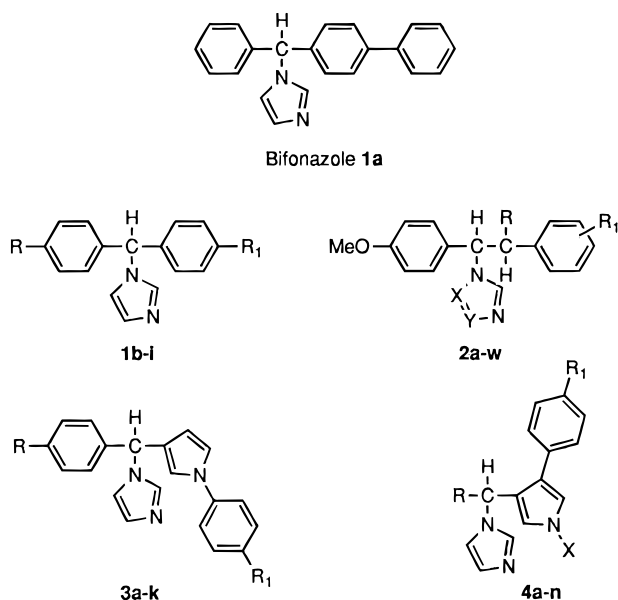
<sup>‡</sup> Dipartimento Farmaco Chimico Tecnologico.

<sup>§</sup> Centro Interdipartimentale per lo Studio dei Sistemi Biomolecolari.

<sup>||</sup> Dipartimento di Studi Farmaceutici.

<sup>⊥</sup> Dipartimento di Studi Chimica e Tecnologia delle Sostanze Biologicamente Attive.

<sup>®</sup> Abstract published in *Advance ACS Abstracts*, January 15, 1996.

**Chart 1.** Azole Antifungal Agents Used in the CoMFA Study

stances where the immune system is compromised to a great extent (AIDS pathology, major surgery interventions), and the side effects (inhibition of the host P-450<sub>DM</sub>) due to overdosage of the azole compounds may eventually cause the death of patients.<sup>10,11</sup>

Although P-450<sub>DM</sub> enzymes have been purified from different sources (*Saccharomyces cerevisiae*,<sup>12</sup> *Candida albicans*,<sup>13</sup> rat liver,<sup>14</sup> and pig liver<sup>15</sup>), no experimental structural information on the active site of the enzymes is yet available. This kind of information is of fundamental importance, and in order to improve the specificity of the antifungal drugs, theoretical and computational methods are being extensively used in the pursuance of this task. In particular, computer models of P-450<sub>DM</sub> from *S. cerevisiae* and *C. albicans* (based on primary sequence analyses and modeling by homology) have been developed<sup>16,17</sup> and, with the help of docking experiments, will probably help to get some information about the binding mode of the active site.<sup>18</sup> However, these models have yet to be proven reliable for accurately describing the 3D-structural features of the enzymes or for reproducing the known trends in inhibitory activity as well as the binding capabilities of both substrates and inhibitors. An alternative and indirect approach which focuses mainly on structural and physicochemical properties of both active and inactive compounds could also be useful in identifying structure-activity relationships helpful to design new and more specific fungicides and, eventually, to understand the enzyme active site topography.

Herein, we describe a 3D-quantitative structure-activity relationship (3D-QSAR)<sup>19</sup> study of several azole antifungal agents previously synthesized by us<sup>20-25</sup> and found to be active *in vitro* against *C. albicans*, a widespread opportunistic fungal pathogen that causes superficial and systemic mycoses in human and animal hosts.<sup>26</sup> The compounds that have been studied are shown in Chart 1. They belong to different structural classes related to bifonazole (**1a**) which is one of the antimycotic drugs of current clinical use.<sup>27</sup> The comparative molecular field analysis (CoMFA)<sup>28</sup> technique has been applied to develop a model able to explain and

predict the activity of bifonazole-like *C. albicans* P-450<sub>DM</sub> inhibitors helpful to design new and more selective fungicides.

Following a more theoretical approach, efforts have also been directed toward the development of a model of the complex between the enzymatic protoporphyrin system and azole inhibitors with the aim to bring up to date other qualitative interaction models proposed in the past,<sup>29,30</sup> and the results of this study will be reported independently in due course.

## Methods

**Biological Data.** Tables 1 and 2 list the structures and the observed and calculated biological activity values of compounds **1a-g**, **2a-p**, **3a-h**, **4a-i** and **1h,i**, **2q-v**, **3i-k**, **4j-n**, forming the training set used to derive the CoMFA models and the set used to test the predictivity of the models themselves, respectively. The antimycotic activity against *C. albicans* was evaluated by means of the minimal inhibitory concentration (MIC) using the serial dilution test in a liquid nutrient medium. The MIC is defined as the lowest concentration ( $\mu\text{g/mL}$ ) of tested substance at which there is no macroscopic colonial growth in comparison with a blank experiment after the preset incubation time. MIC<sub>90</sub> refers to the MIC for 90% of strains, standardized on bifonazole as the control. In this CoMFA study, the biological activity of each compound has been expressed as  $-\log(\text{MIC}_{90}(\text{compd})/\text{MIC}_{90}(\text{bifonazole}))$ . Consequently, all the activity values are in the range of -2.4 (less active compounds) to 0.9 (more active compounds). The five derivatives which have been found to be "inactive" (see Tables 1 and 2) were arbitrarily assigned an activity value equal to 50% of that of the compounds reported as the less active in their respective structural classes.<sup>20-25</sup> Although such data might represent a disturbing source of noise, it is, nevertheless, true that the exclusion of a non-negligible number of observations would imply a serious loss of information.<sup>31</sup> Furthermore, although the activity data refer to racemic or diastereomeric mixtures, they have been used in this CoMFA study on the basis of examples in the literature where analogous decisions have been made in dealing with mixtures of diastereoisomers.<sup>32</sup>

**Molecular Modeling.** All the computational work was performed on Silicon Graphics computers (Personal Iris 4D/35, Indigo Entry 4000, Power Series III 4D/480, and Challenge XL).

It is well known that the biological activity of chiral compounds is usually due to one of the enantiomers. Due to this fact and taking into account the presence of at least one asymmetric carbon atom common to all the compounds considered in this study, it was arbitrarily decided to model the *R* enantiomer of bifonazole and construct all the other inhibitors according to this initial choice. This decision can be justified on the basis that intramolecular distances and bond angles do not depend on the asymmetry of any single carbon atom and, consequently, the computational results are also independent of this choice. Further, as already noted, the biological evaluation of all the inhibitors including bifonazole, the reference standard, was carried out using racemic mixtures.

To our knowledge, no experimental data are available on the binding geometry of bifonazole or the other compounds. Although there is no *a priori* reason why a unique binding mode should be favored, it is reasonable to assume that the active site of a target enzyme will bind structurally related compounds in a similar manner. A consistent model that is derived in this way without increasing the complexity due to the introduction of multiple binding modes would be preferred because it would carry the fewest assumptions.<sup>33</sup> For this reason, an exhaustive conformational search was carried out on (*R*)-bifonazole, and the remaining compounds in Chart 1 could be correlated to the results of this search by analogy. The program PCMODEL (MMX force field)<sup>34</sup> which responds well to extended  $\pi$ -electron systems<sup>35</sup> was used to derive optimal coordinates for the *R* stereoisomer of bifonazole. A

**Table 1.** Observed and Calculated *in Vitro* Inhibitory Activity Values of the Compounds Forming the "Training Set" (Alignment Rule II)

compd	R	R <sub>1</sub>	X	Y	-log(MIC <sub>90</sub> (compd)/MIC <sub>90</sub> (bifonazole))		
					obsd <sup>a</sup>	calcd <sup>b</sup>	diff <sup>c</sup>
1a					0.00	-0.15	0.15
1b	H	1-pyrrolyl			0.60 <sup>d</sup>	0.63	-0.03
1c	H	NO <sub>2</sub>			-0.30 <sup>d</sup>	-0.19	-0.11
1d	CH <sub>3</sub>	1-pyrrolyl			0.90 <sup>d</sup>	0.95	-0.05
1e	CH <sub>3</sub>	2,4-Cl <sub>2</sub> -BzNH			0.00 <sup>d</sup>	0.12	-0.12
1f	Cl	NO <sub>2</sub>			0.00 <sup>d</sup>	-0.21	0.21
1g	CH <sub>3</sub>	NO <sub>2</sub>			0.30 <sup>d</sup>	-0.02	0.32
2a	H	4-Cl	CH	CH	-0.60	-0.84	0.24
2b	H	2,4-Cl <sub>2</sub>	CH	CH	-0.60	-0.86	0.26
2c	H	4-NH <sub>2</sub>	CH	CH	-0.30	-0.16	-0.14
2d	H	3-(1-pyrrolyl)	CH	CH	-1.80	-1.85	0.05
2e	H	4-Cl	CH	N	-1.80	-1.76	-0.04
2f	H	2-Cl	CH	CH	-1.80	-1.76	-0.04
2g	H	3-F	CH	CH	-1.80	-2.07	0.27
2h <sup>e</sup>	H	2-NO <sub>2</sub>	CH	CH	-2.10	-2.04	-0.06
2i	H	4-OCH <sub>3</sub>	CH	N	-1.80	-1.87	0.07
2j	H	2-(1-pyrrolyl)	CH	CH	-0.90	-0.77	-0.13
2k	H	4-NO <sub>2</sub>	CH	CH	-1.50	-1.12	-0.38
2l	H	4-OCH <sub>3</sub>	CH	CH	-0.90	-0.86	-0.04
2m	H	4-Cl	N	CH	-1.50	-1.43	-0.07
2n	C <sub>2</sub> H <sub>5</sub>	4-NO <sub>2</sub>	CH	CH	-0.90	-0.99	0.09
2o	2,4-Cl <sub>2</sub> -Bn	4-OCH <sub>3</sub>	CH	CH	-1.50	-1.40	-0.10
2p	2,4-Cl <sub>2</sub> -Bn	4-Cl	N	CH	-1.80	-1.87	0.07
3a	H	H			-0.60	-0.38	-0.22
3b	CH <sub>3</sub>	H			0.00	-0.04	0.04
3c	Cl	Cl			-0.60	-0.29	-0.31
3d	F	Cl			-0.30	-0.35	0.05
3e	H	Cl			0.30	-0.26	0.56
3f	CH <sub>3</sub>	F			-0.30	-0.20	-0.10
3g	Cl	F			-0.30	-0.43	0.13
3h	H	F			-0.60	-0.41	-0.19
4a	Ph	Cl	H		0.30	0.21	0.09
4b	Ph	Cl	CH <sub>3</sub>		0.00	-0.11	0.11
4c	Ph	F	H		0.00	0.14	-0.14
4d <sup>e</sup>	Ph	OCH <sub>3</sub>	2,4-Cl <sub>2</sub> -Bn		-1.80	-1.80	0.00
4e	Ph	H	2,4-Cl <sub>2</sub> -Bn		-1.50	-1.69	0.19
4f <sup>e</sup>	Ph	Cl	2,4-Cl <sub>2</sub> -Bn		-1.80	-1.59	-0.21
4g	1-naphthyl	H	H		-0.90	-0.85	-0.05
4h	2-naphthyl	H	H		-0.90	-1.21	0.31
4i <sup>e</sup>	2-naphthyl	H	CH <sub>3</sub>		-2.40	-2.05	-0.35

<sup>a</sup> Experimental data taken from refs 20–25. <sup>b</sup> Values calculated according to the calibration model based on alignment II. <sup>c</sup> Difference between observed and calculated values. <sup>d</sup> Unpublished results. <sup>e</sup> "Inactive" compounds which were assigned an activity value equal to 50% of that of the compounds reported as the less active in their respective structural class.

**Table 2.** Observed *in Vitro* Inhibitory Activity Values of the Compounds Forming the "Test Set" (Alignment Rule II)

compd	R	R <sub>1</sub>	X	Y	obsd <sup>a</sup> -log (MIC <sub>90</sub> (compd)/ MIC <sub>90</sub> (bifonazole))
1h	Cl	1-pyrrolyl			0.30 <sup>b</sup>
1i	H	NH <sub>2</sub>			-0.30 <sup>b</sup>
2q	H	3-Cl	CH	CH	-1.50
2r	H	2-F	CH	CH	-1.80
2s	H	4-F	CH	CH	-1.20
2t	C <sub>2</sub> H <sub>5</sub>	4-Cl	N	CH	-1.50
2u	C <sub>2</sub> H <sub>5</sub>	4-Cl	CH	N	-1.80
2v	2,4-Cl <sub>2</sub> -Bn	4-Cl	CH	CH	-1.20
3i	F	H			-0.30
3j	CH <sub>3</sub>	Cl			0.00
3k	F	F			0.00
4j	Ph	CH <sub>3</sub>	CH <sub>3</sub>		-0.60
4k	Ph	H	CH <sub>3</sub>		-0.60
4l <sup>c</sup>	Ph	CH <sub>3</sub>	2,4-Cl <sub>2</sub> -Bn		-1.80
4m	Ph	F	CH <sub>3</sub>		-0.60
4n	1-naphthyl	H	CH <sub>3</sub>		-1.50

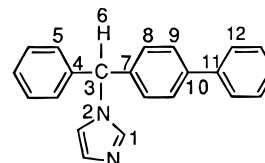
<sup>a</sup> Experimental data taken from refs 20–25. <sup>b</sup> Unpublished results. <sup>c</sup> See footnote e in Table 1.

conformational analysis of bifonazole (statistical method) was then performed with the program BKM,<sup>36</sup> which implements a generalized MM2 force field while randomly varying the rotatable bonds as reported in Table 3. Even though this procedure gives no absolute guarantee that the global mini-

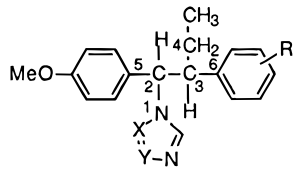
**Table 3.** Investigated Torsions,<sup>a</sup> Increments of Rotation, Ranges of Investigation, and Geometry of the Lowest Energy Conformer of Bifonazole (1a) as Calculated with Different Programs<sup>b</sup>

	investigated torsions (deg)			
	τ <sub>1</sub>	τ <sub>2</sub>	τ <sub>3</sub>	τ <sub>4</sub>
increment	30	30	30	15
range	0 ÷ 360	-90 ÷ 90	-90 ÷ 90	-30 ÷ 30
PCMODEL (MMX f.f.)	-105	31	1	-40
BKM (MM2 <sub>gen</sub> f.f.)	-109	30	2	-43
MNDO	-145	32	30	-90
AM1	-157	27	20	-40
PM3	-160	27	19	-47

<sup>a</sup> τ<sub>1</sub> = τ(H6,C3,N2,C1); τ<sub>2</sub> = τ(H6,C3,C4,C5); τ<sub>3</sub> = τ(C8,C7,C3,H6); τ<sub>4</sub> = τ(C12,C11,C10,C9). <sup>b</sup> PCMODEL and BKM: molecular mechanics programs.<sup>34,36</sup> MNDO, AM1, and PM3: semiempirical Hamiltonians implemented in MOPAC.<sup>38</sup>



mum has been located, the following reasons give us confidence about the reliability of the geometry obtained. First, the

**Table 4.** Comparison between Experimental and Calculated Structural Features of Compounds **2u,w**


compd	dihedral angles (deg)		
	N1-C2-C3-C4	C6-C3-C2-C5	angle between the phenyl ring planes
<b>2w</b> <sup>a</sup>	180	171	13
<b>2u</b> <sup>b</sup>	-177	-179	3

<sup>a</sup> R = 4-Br. Experimental values determined by X-ray crystal structure analysis. <sup>b</sup> R = 4-Cl. Theoretical values calculated by molecular modeling studies.

statistical search procedure favors the low-energy regions of the conformational space;<sup>37</sup> second, the search was stopped when duplicate geometries were mostly generated and the global minimum structure had been found several times. A detailed description of the conformational analysis procedure can be found in our previous publications.<sup>37</sup> Although many conformers with an energy difference of <3 kcal/mol relative to the global minimum were found, only the lowest energy conformer was used for further studies. Due to the lack of crystallographic data on bifonazole, a further optimization of the geometry obtained from the molecular mechanics calculations was done using semiempirical quantum mechanical methods (MNDO, AM1, and PM3 in MOPAC).<sup>38</sup> The results obtained are in good agreement with those derived from the molecular mechanics calculations (Table 3) and gave confidence on the reliability of the calculated geometry for bifonazole. Optimal coordinates for each of the other molecules forming the training and test sets were obtained by carrying out "atom by atom" modifications of the lowest energy conformer of (*R*)-bifonazole followed by an interactive energy minimization of each structure in PCMODEL. Compounds **2a-w**, which have an extra sp<sup>3</sup> carbon atom than bifonazole, were easily built by inserting this group into the lowest energy conformer of bifonazole and minimizing the strained geometry so obtained. The added C2-C3 rotatable bond (see Table 4) was then scanned by increments of 120° affording its preferred arrangement where the phenyl rings have an *anti* disposition. Considering the high flexibility of the molecules forming the training set and their structural similarity to bifonazole, the Sybyl (version 6.0)<sup>39</sup> MULTIFIT procedure was utilized to fit the 3D-geometries of **1b-d,f,g**, **2a-m**, **3a-h**, and **4a-c,g-i** with the lowest energy conformer of bifonazole instead of performing extensive, time-consuming, conformational searches on them. Inhibitors **1e**, **2n-p**, and **4d-f** (Chart 1) present extra torsional degrees of freedom with respect to bifonazole. Therefore, these derivatives were not superimposable to bifonazole by simply applying to them the MULTIFIT procedure described above, and a partial statistical conformational search was then performed with BKM on the few extra rotatable bonds in order to find their lowest energy orientation.

The relevance of the molecular modeling studies was tested using compound **2w** (R = 4-Br, X = CH, Y = N; C2(*R*), C3(*R*) stereoisomer; the atomic numbering is given in Table 4) as a reference structure. This compound was not included in the present CoMFA study, and its 3D-structure is secured by X-ray crystallography.<sup>21</sup> A comparison of selected torsion angles with those of modeled compounds such as **2u** (C2(*R*), C3(*R*) stereochemistry) shows (see Table 4) excellent agreement, gives confidence to the use of molecular mechanics calculations for determining the geometries of compounds **1-4**, and once more confirms the high quality of the PCMODEL/BKM force fields for these types of structures.

**3D-QSAR Methodology.** CoMFA calculations were performed using the QSAR module of Sybyl and with the following characteristics: The grid in which the molecules were embedded was regularly spaced (1 Å) with dimensions of 18 × 20 ×

22 Å (these values were determined by an automatic procedure performed by the Sybyl-CoMFA routine). Steric and electrostatic interaction energies were calculated using a carbon sp<sup>3</sup> probe atom with a +1 charge, a distance-dependent dielectric constant (1/*r*), and an energetic cutoff of 30 kcal/mol with no electrostatic interactions at sterically bad contacts. The same 3D-grid was used in all the CoMFA studies.

Regression analyses were done using the Sybyl implementation of the PLS<sup>40</sup> algorithm, initially with cross-validation<sup>41</sup> (the leave-one-out technique) to reduce the probability of obtaining chance correlations and 10 principal components (PCs). The number of groups of cross-validation was set equal to the number of components of the training set. The optimal number of latent variables (components) to be used in conventional analyses was chosen on the basis of the highest cross-validated *r*<sup>2</sup> (*r*<sup>2</sup><sub>cv</sub>) value, the smallest standard error of prediction (SEP), and the minimum number of components. To improve the signal-to-noise ratio, all leave-one-out calculations were performed selecting a 2.0 kcal/mol energy column filter (the so-called minimum sigma option or field variance at each grid point was used for this purpose). The steric and electrostatic field columns were weighted according to the COMFA-STD default scaling option. In this method a field is considered as a whole and every CoMFA variable is affected by the overall field mean and standard deviation. Final PLS (non-cross-validated models) calibration equations were then derived using the optimal number of components so identified.

To assist selection among various 3D-QSAR calibration equations (models) and to test their utility as predictive tools, an external set (the so-called test set) of compounds with known activities not used in model generation was predicted. The predictive *r*<sup>2</sup> based only on molecules from the test set is normally reported as the most appropriate parameter to evaluate the predictive power of a CoMFA model. Predictive *r*<sup>2</sup> is calculated using the following equation:

$$\text{predictive } r^2 = 1 - (\text{"press"}/\text{SD})$$

where SD is the sum of the squared deviations between the actual activities of the compounds in the test set and the mean activity of the training set compounds and "press" is the sum of the squared deviations between predicted and actual activities for every compound in the test set. It is obvious from the equation that prediction of the mean value of the training set for every member in the test set yields a predictive *r*<sup>2</sup> = 0, while negative values are possible when the predictions are worse than predicting the mean value of the training set. This procedure was followed to evaluate the predictive ability of our CoMFA models.

As a further attempt to validate the best CoMFA model obtained, the bootstrap validation method<sup>41</sup> was used as implemented in Sybyl. This technique is used to estimate the stability of the parameters (mean and standard deviation) associated with the statistical models.

CoMFA coefficient contour maps of the coefficients of each grid point were also generated by following the standard procedure in Sybyl. These maps show lattice points where the QSAR strongly associates changes in steric and electrostatic field values with changes in biological activity in order to obtain chemical information.

**CoMFA Models I and II.** CoMFA was used to examine the correlation between calculated physicochemical properties (steric and electrostatic) and measured *in vitro* inhibitory activities of a training set of 40 inhibitors. The "alignment rule", that is, the superimposition of the molecular models within a 3D-fixed lattice, is one of the most important input variables in CoMFA. For this purpose, flexible compounds are by far the most difficult to model. To define the alignment rules for a flexible training set, one can use a variety of methods that are generally dependent on whether or not crystallographic data are available. Since no X-ray structural information for any of the enzyme-inhibitor complexes is available, rather than using the more common "field-fit" procedure, a more reliable conformational search was undertaken to elicit these data.<sup>42</sup> Except for the model of lanosterol 14α-demethylase of *S. cerevisiae*, built by Richards and co-

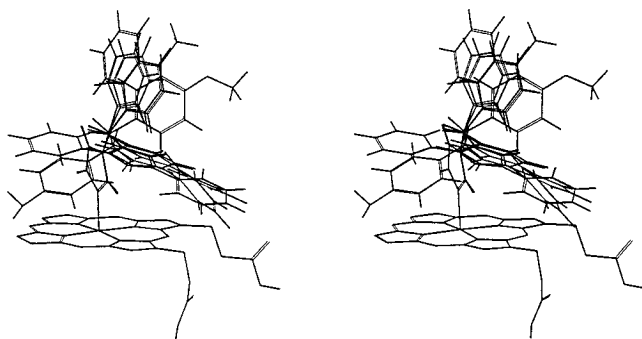


**Figure 1.** Stereoview of the superimposition of compounds **1a,b**, **2c**, **3b**, and **4f** according to alignment rule I. Bifonazole (**1a**; template) is complexed to the porphyrin system, which is also shown in the figure (partially for clarity). In the upper part of the figure, the poor superimposition of the phenyl rings, common to all the compounds, is evident.

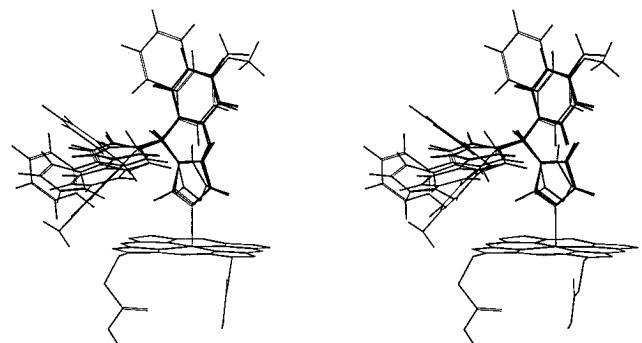


**Figure 2.** Stereoview of the superimposition of compounds **1a,b**, **2c**, **3b**, and **4f** according to alignment rule II. Bifonazole (**1a**; template) is coordinated to the porphyrin system which is also shown in the figure (partially for clarity). It is evident that while the azole moieties of different compounds, which are linked to iron, are not perfectly superimposed, the phenyl rings common to all the compounds show a quite good matching.

workers using modeling by homology and whose 3D-structure is still unpublished, only qualitative information about the binding mode of azole antifungal agents is deducible from the literature.<sup>29</sup> From this body of work, there is a consensus that three salient features characterize the enzyme-binding site: (1) a porphyrin iron atom coordinating the unsubstituted azole N atom, (2) a largely hydrophobic binding pocket, and (3) a polar hydrophilic region, where polar group(s) of the substrate can interact with a histidine residue, the propionate side-chains of heme, or solvent molecules. Therefore, it was decided to investigate two different alignments. First, the molecules forming the training set were aligned by superimposition of their azole rings in the alignment named I. For the second alignment (named II), 11 heavy atoms (azole and phenyl groups linked to the asymmetric carbon atom) common to all the molecules were superimposed by performing rigid-body, least-squares fittings. Alignments I and II are shown in Figures 1 and 2, respectively, where compounds **1a,b**, **2c**, **3b**, and **4f** are properly superimposed. In these figures, bifonazole is coordinated to the heme moiety which is also partially shown. The structural properties of the bifonazole-porphyrin complex (the ligand, cysteinyl S, is not shown in the figures for the sake of simplicity) have been studied by molecular mechanics calculations.<sup>43</sup>

The activities of the studied compounds (see Table 1) were distributed across a range of 3.3 log units going from -2.4 to 0.9 and centered on bifonazole (0.0). Table 5 reports the statistical results of the cross-validated PLS-CoMFA experiments according to alignment rules I and II. The statistics of the final "best correlation" models with the optimal number of components for the two models are given in Table 6.

**Test Set.** The test set consisted of 16 molecules (**1h,i**, **2q-v**, **3i-k**, **4j-n**), which are representatives of all the structural

**Table 5.** Statistics of the Cross-Validated CoMFA Analyses Based on Alignments I and II<sup>a</sup>

principal components	alignment I		alignment II	
	$r^2_{cv}$	SEP	$r^2_{cv}$	SEP
1	0.29	0.73	0.28	0.72
2	0.39	0.68	0.43	0.65
3	0.45	0.65	0.50	0.62
4 <sup>b</sup>	0.52	0.62	0.52	0.61
5	0.48	0.66	0.54	0.61
6 <sup>c</sup>	0.47	0.67	0.57	0.60
7	0.46	0.69	0.58	0.60
8	0.49	0.68	0.60	0.60
9	0.49	0.69	0.60	0.61
10	0.49	0.70	0.60	0.62

<sup>a</sup> Minimum  $\sigma = 2.0$ ; number of cross-validation runs = 40.

<sup>b</sup> Optimal number of principal components found for alignment I.

<sup>c</sup> Optimal number of principal components found for alignment II.

classes of inhibitors whose activities spanned 2 orders of magnitude covering a range of 2.1 log units (from -1.8 to 0.30). These derivatives were chosen among active and inactive compounds to maximize a uniform sampling of biological activity. The conformational choices and the alignment rules for the test set molecules were constrained by the CoMFA models themselves since both the test set molecules and the training set ones belong to the same structural classes. All predicted activities for the test set molecules were calculated using the optimal CoMFA models established for both alignments I and II. The predictive power results of the two non-cross-validated calibration models on the test set are summarized in Tables 6 and 7. The prediction statistics are given in Table 6, and Table 7 reports the activities based on these values.

Supplementary material containing Sybyl databases for training set and test set compounds aligned according to rules I and II is available from the authors upon request.

## Results and Discussion

One of the variables in the CoMFA procedure is the calculation of the point charges. However, from recent publications there is strong evidence to suggest that in CoMFA the overall influence of the point charges is not sensitive to the method of how these are calculated.<sup>32</sup> Therefore, the partial atomic charges for all the molecules were computed with Sybyl using the GAST-HUCK method of this program and used without further refinement.

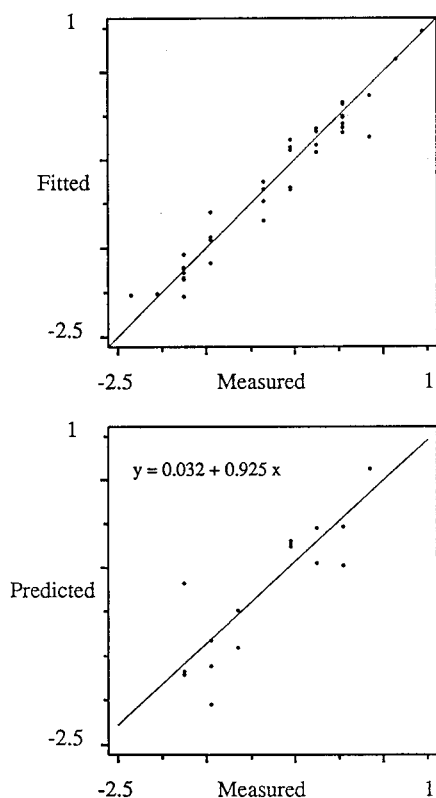
The cross-validated analysis using the 40 compounds in the training set, based on alignment I, identified four optimal components out of 10 (Table 5) with a cross-validated  $r^2$  value of 0.52 and a SEP of 0.62 log unit. The corresponding non-cross-validated analysis (four components) resulted in a conventional correlation coefficient ( $r^2$ ) value of 0.89 (Table 6). The model thus generated is able to account for 89.4% of the total variance in inhibitory activity of the 40 training set compounds with a standard error of estimate (SEE) of 0.29 log unit ( $F$ -test value = 74.16). The contributions of steric and electrostatic fields to the QSAR equation were respectively 59.8% and 40.2%.

Alignment II yielded better cross-validated results ( $r^2_{cv} = 0.57$ , SEP = 0.60 log unit) (Table 5) and conventional results ( $r^2 = 0.95$ ,  $F$ -test value = 103.20) (Table 6). In this second case the optimal number of components found was 6. The corresponding calibrated model satisfies 94.9% of the total variance in inhibitory activity found in the training set with a SEE of 0.20 log unit. In this model, the contributions of steric and electrostatic fields to the QSAR equation are 58.4% and 41.6%,

**Table 6.** Statistics of the Calibration CoMFA Models Based on Alignments I and II, Including Predictive  $r^2$  for the Entire Test Set ( $r^2_{\text{pred}}$ ) and after the Exclusion of the Outlier **2r** ( $r^2_{\text{pred}} - \mathbf{2r}$ )

alignment method	$r^2$	SEE	F-test	$r^2_{\text{pred}}$	$r^2_{\text{pred}} - \mathbf{2r}$	steric and electrostatic contributions (%)	$r^2_{\text{boot}}^a$	SEE $_{\text{boot}}^a$
I	0.89	0.29	74.16	0.63	0.69	59.8, 40.2		
II	0.95	0.20	103.20	0.69	0.82	58.4, 41.6	$0.97 \pm 0.01$	$0.16 \pm 0.10$

<sup>a</sup> Results of the bootstrapped analysis (30 samplings, minimum  $\sigma = 2.0$ ).

**Figure 3.** Fitted predictions vs measured  $p(\text{MIC}_{90}(\text{compd})/\text{MIC}_{90}(\text{bifonazole}))$  for the CoMFA analysis of the 40 lanosterol  $14\alpha$ -demethylase inhibitors aligned according to rule II. The model was derived using SIX principal components yielding a cross-validated  $r^2 = 0.57$ . (Top) Predicted vs measured values of  $p(\text{MIC}_{90}(\text{compd})/\text{MIC}_{90}(\text{bifonazole}))$  for the test set of 16 inhibitors using the model based on alignment II to generate predictions. (Bottom) Corresponding curve fit equation.

respectively. A high bootstrapped (30 samplings)  $r^2$  value of  $0.97 \pm 0.01$  with a correspondingly small SEE ( $0.16 \pm 0.10$  log unit) adds a high degree of confidence to this analysis. The upper part of Figure 3 depicts a plot of observed vs calculated *in vitro* inhibitory activities of compounds **1a–g**, **2a–p**, **3a–h**, and **4a–i** using the optimal non-cross-validated model based on alignment II.<sup>44</sup>

As already noted, the 16 compounds **1h,i**, **2q–v**, **3i–k**, and **4j–n** (test set) were used to evaluate the predictive power of the CoMFA models I and II. Tables 6 and 7 show that the predictions of the model based on alignment II are improved by exclusion of compound **2r**, resulted as an outlier probably because only two 3-substituted compounds were used to derive the CoMFA model. On the other hand, **2d,g** were the only biologically active ones among the 3-substituted derivatives already synthesized. As in the calibration experiments, alignment II also gives the best predictive ability with an  $r^2_{\text{pred}}$  of 0.82 for the 15 compounds in the test set ( $r^2_{\text{pred}} = 0.69$  for the full test set). From Table 7, it can be seen that the activities of all the examined compounds are predicted within 0.57 log unit of their

**Table 7.** Measured Activities [ $-\log(\text{MIC}_{90}(\text{compd})/\text{MIC}_{90}(\text{bifonazole}))$ ], Differences between Measured and Predicted Activities, and Average Absolute Errors of Predictions for the Test Set Molecules Using Alignments I and II

compd	measd	alignment		compd	measd	alignment	
		I	II			I	II
<b>1h</b>	0.30	-0.15	-0.31	<b>3i</b>	-0.30	0.07	0.17
<b>1i</b>	-0.30	-0.50	-0.23	<b>3j</b>	0.00	0.33	0.05
<b>2q</b>	-1.50	0.39	0.57	<b>3k</b>	0.00	0.40	0.50
<b>2r</b>	-1.80	-0.88	-1.10	<b>4j</b>	-0.60	-0.42	-0.35
<b>2s</b>	-1.20	-0.15	-0.19	<b>4k</b>	-0.60	-0.47	-0.38
<b>2t</b>	-1.50	-0.37	-0.16	<b>4l</b>	-1.80	0.09	-0.07
<b>2u</b>	-1.80	-0.59	-0.10	<b>4m</b>	-0.60	-0.56	0.32
<b>2v</b>	-1.20	0.20	0.22	<b>4n</b>	-1.50	-0.40	0.13

Average Absolute Errors of Predictions

	alignment	
	I	II
for 16 compounds	0.37	0.30
for 15 compounds ( <b>2r</b> excluded)	0.34	0.25

actual inhibitory activities (excluding outlier **2r** which is badly predicted and shows a residual of 1.10 log units) with an average absolute error of 0.25 log unit across a range of 2.1 log units (the average absolute error value is raised to 0.30 log unit if all 16 compounds are used in the analysis). Alignment I gave slightly poorer predictive results ( $r^2_{\text{pred}} = 0.63$  for the full test set which improves to 0.69 by excluding compound **2r**) as shown in Table 6. This model mispredicted the activities of the test set molecules by as much as 0.88 log unit (for **2r**) with an average absolute error of 0.37 log unit in predictivity (0.34 log unit for 15 compounds). The predictive power results are shown in the lower part of Figure 3 which reports a plot of measured vs predicted *in vitro* inhibitory activities of the 16 compounds using the non-cross-validated model based on alignment II.

Since at least two compounds for each of the structurally different families of inhibitors are comprised in the test set of molecules and due care was made to ensure the biological activity got sampled in a uniform way, we are confident that the predictive power of the chosen CoMFA models was correctly evaluated.

The results given in Tables 5–7 strongly support the alignment rules for inhibitors **1a–i**, **2a–v**, **3a–k**, and **4a–n**. Alignment II, which takes into account not only the very important superimposition of the azole moieties but also the fitting of the phenyl rings common to all the compounds, expresses better predictive power than alignment I. The binding mode of azole-type inhibitors of aromatase, an enzyme belonging to the cytochrome P-450 suprafamily, is reported<sup>27</sup> to have a rigid and well-defined binding geometry that has the azole moiety bound to the protoporphyrin iron atom with the N–C bond of the azole moiety eclipsing one of the Fe–N bonds of the porphyrin system. On the basis of this model, Fromtling<sup>27</sup> has been able to correlate the differences observed in the biological activity of the

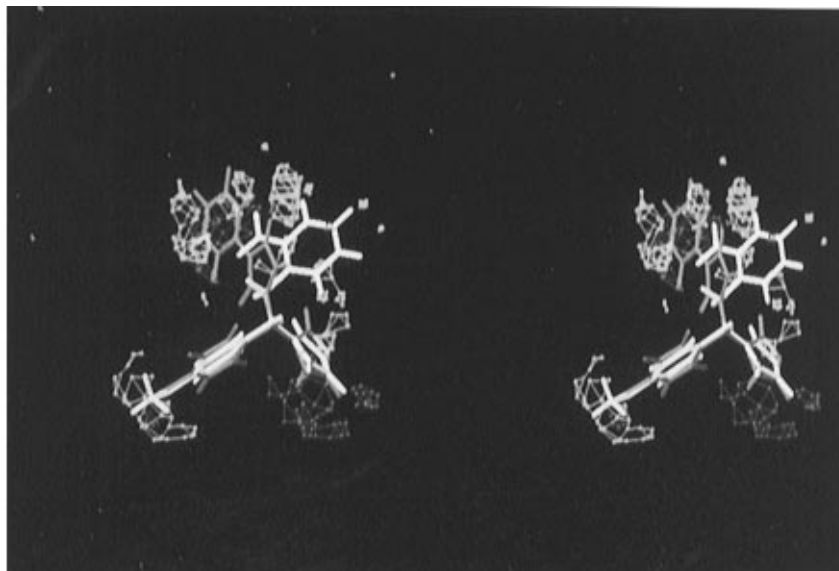


**Figure 4.** CoMFA electrostatic STDEV\*COEFF contour plot from the analysis based on alignment rule II. Negative charge not favored areas (contribution level 88%) are represented by red polyhedra. Negative charge-favored areas (contribution level 12%) are represented by blue polyhedra. Active compound **2h** is represented as a green structure. Less active compound **3g** is represented as a yellow structure.

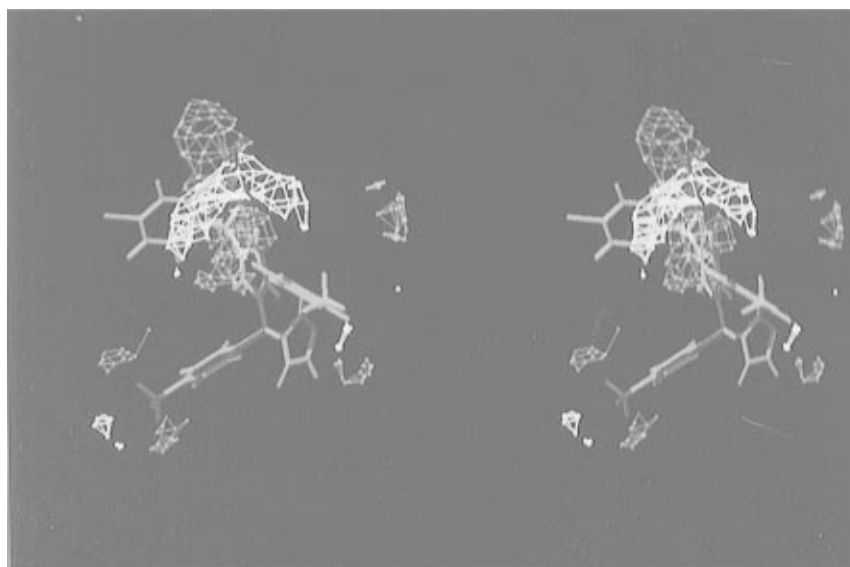


**Figure 5.** CoMFA steric STDEV\*COEFF contour plot from the analysis based on alignment rule II. Sterically favored areas (contribution level 90%) are represented by green polyhedra. Sterically not favored areas (contribution level 10%) are represented by yellow polyhedra. The more active compound **1d** and the less active compound **4d** are also represented as blue and a red structure, respectively.

various inhibitors. In Figure 1, for example, is shown alignment I which simulates this binding mode leaving the phenyl groups of the ligands relatively free in 3D-space. However, in Figure 2, which shows alignment II, the phenyl groups are not free in 3D-space but superimposed to emphasize a pharmacophoric relevance. This latter model implies a more flexible geometry of coordination in which a small torsional freedom around the coordination bond is still present. If this is the real binding mode, then in order to be highly active as antifungal agents the ligands are expected to optimize their relevant binding interactions (most likely hydrophobic) with the enzyme cavity.

The CoMFA steric and electrostatic fields for the analysis based on alignment II are shown as contour maps in Figures 4 and 5. The field values were calculated at each grid point as the scalar product of the associated QSAR coefficient and the standard deviation of all values in the corresponding column of the data

table (STDEV\*COEFF) and always plotted as the percentage of contribution to the QSAR equation. These surfaces are to be considered as a representation of the lattice points, where differences in field values are strongly associated with differences in inhibitory potency. Though the interpretation of these maps is primarily intuitive and highly subjective, the absence of the lattice points does not mean that a given pharmacophore element has no influence on the biological activity. It can also indicate that all the examined compounds exert the same steric and/or electrostatic influence in a certain area or, as suggested by Cramer,<sup>28</sup> can help to delineate the less explored volume of a lattice. In Figure 4 are shown the electrostatic contour maps. The red contours represent regions of decreased tolerance for positive charge (12% contribution), while the blue contours represent regions of decreased toler-



ance for negative charge (88% contribution). In Figure 5 (steric contour maps) the yellow contours represent regions of low steric bulk tolerance (10% contribution), while the green contours represent regions of high steric tolerance (90% contribution).

As can be seen in Figure 5, green polyhedra running parallel, mostly on the lower side, to the hydrogen atoms of the conjugated aromatic moiety (biphenyl or pyrrol-ylphenyl) of the most active compounds such as **1a–g**, **3b**, and **4a–c** could also indicate favorable steric interactions of these structural elements with a large hydrophobic pocket in the active site. In Figure 5, a yellow contour region which extends roughly perpendicular to the previously described green region and accommodates the aromatic moieties of the less active compounds, like **4d**, is visible. The compounds which have an extra CH<sub>2</sub> group between the imidazole and the aromatic residues (**2a–v**) are less active because their aromatic residues are extended away from the favored region of interaction. According to this binding hypothesis, some small red polyhedra (Figure 4), indicating areas where high electron density within the ligands enhances affinity, are overlapping with the  $\pi$ -aromatic electron density of the most active compounds. Small green contour regions, indicating favorable steric interactions with a possible *para*-substituent of the phenyl group located here (see compound **1c**), are shown in the lower left corner of Figure 5. A small steric yellow region external to the green region also suggests that the dimensions of these substituents can not be too large or it will render the compound inactive (*i.e.*, **4g–i**). In Figure 4 is shown that in the same area, overlapping with the green polyhedra, a red electrostatic contour region is present suggesting that a negative charge is preferred on the *para*-substituents of the phenyl group. In the upper right part of Figure 5, a small green region that is almost superimposable to the small red electrostatic spot shown in Figure 4 can be seen. It corresponds to the spatial position that tends to be occupied by the R' substituent present in the more active compounds **2**, and therefore, an expression in this area is associated with enhanced activity (see the activities of compounds **2n,l** compared to the activity of the other compounds **2**). With respect to the azole moiety, a green steric contour (Figure 5) and an electrostatic blue contour (Figure 4) are present. Both these regions express the preference of an imidazole over a triazole group in the active site. This is also supported by the results listed in Table 1, which consistently show the imidazole derivatives to be more active than the triazoles. Furthermore, the large electrostatic blue region which is appreciable in Figure 4 in the "conjugated aromatic" region (left upper side in Figure 4) represents a decrease in activity if there are electron-withdrawing substituents present (for example, the NO<sub>2</sub> group in compound **2h**).

## Conclusions

The CoMFA 3D-QSAR method has been applied to a set of antifungal agents active against *C. albicans*. The studied compounds belong to chemically diverse families of imidazole and triazole derivatives, able to inhibit lanosterol 14 $\alpha$ -demethylase enzyme, which have been synthesized in our laboratories. This CoMFA study successfully explains the structure–activity relation-

ships in a set of 40 inhibitors. It also predicts accurately the biological activity of 15 molecules not used in deriving the CoMFA model itself. Obviously, the results of this investigation will be of fundamental importance for future synthetic efforts in this area in that they offer useful suggestions about how to design new inhibitors. Moreover, the alignment method II utilized to derive the predictive CoMFA model gives an insight into a possible binding mode between these inhibitors and the protoporphyrin system of the target enzyme.

**Acknowledgment.** Financial support of this research by the EEC Programme "Human Capital and Mobility" (Contract No. ERBCHRXCT 920027) and by the Italian CNR is gratefully acknowledged. A.T. wishes to thank the EEC Commission, Programme "Human Capital and Mobility", for a postdoctoral fellowship (1994–1995).

## References

- (1) Partially presented at the NATO ASI School, Metal-ligand interactions: structure and reactivity, Cetraro (Cs), Italy, September 4–16, 1994, and at the Joint Greek-Italian Meeting on Chemistry of Biological Systems and Molecular Chemical Engineering, Ioannina, Greece, December 20–23, 1994.
- (2) *Cytochrome P-450: Structure, Mechanism and Biochemistry*; Ortiz de Montellano, P. R., Ed.; Plenum Press: New York and London, 1986; references cited therein.
- (3) Akhtar, M.; Wright, J. N. A Unified Mechanistic View of Oxidative Reactions Catalysed by P-450 and Related Fe-Containing Enzymes. *Nat. Prod. Rep.* **1991**, *8*, 527–551.
- (4) Banting, L.; Nicholls, P. J.; Shaw, M. A.; Smith, H. J. In *Progress in Medicinal Chemistry*, V. 26; Ellis, G. P., West, G. B., Eds.; Elsevier Science Publishers, B.W.: Amsterdam, 1989; pp 253–298.
- (5) Vanden Bossche, H. In *Sterol Biosynthesis Inhibitors. Pharmaceutical and Agrochemical Aspects*; Berg, D., Plentel, M., Eds.; Ellis Horwood: Chichester, England, 1988; pp 79–119.
- (6) Adams, J. L.; Metcalf, B. W. Therapeutic Consequences of the Inhibition of Sterol Metabolism. In *Comprehensive Medicinal Chemistry*, V. 2; Hansch, C., Sammes, P. G., Taylor, J. B., Eds.; Pergamon Press: Oxford, England, 1990; pp 333–364.
- (7) Hitchcock, C. A.; Dickinson, K.; Brown, S. B.; Evans, E. G. V.; Adams, D. J. Interaction of Azole Antifungal Antibiotics with Cytochrome P-450-Dependent 14 $\alpha$ -Sterol Demethylase Purified from *Candida albicans*. *Biochem. J.* **1990**, *266*, 475–480.
- (8) Yeagle, P. L.; Martin, R. B.; Lala, A. K.; Lin, H. K.; Block, K. Differential Effects of Cholesterol and Lanosterol on Artificial Membranes. *Proc. Natl. Acad. Sci. U.S.A.* **1977**, *74*, 4924–4926.
- (9) Yoshida, Y.; Aoyama, Y. Interaction of Azole Antifungal Agents with Cytochrome P-450<sub>14DM</sub> Purified from *Saccharomyces cerevisiae* Microsomes. *Biochem. Pharmacol.* **1987**, *36*, 229–235.
- (10) Goldman, R. C.; Klein, L. L. Problems and Progress in Opportunistic Infections. In *Annual Reports in Medicinal Chemistry*, V. 29; Bristol, A. J., Ed.; Academic Press, Inc.: San Diego, CA, 1994; pp 155–164.
- (11) Odds, F. C.; Schmid, J.; Soll, D. R. Epidemiology of *Candida* Infections in AIDS. In *Mycoses in AIDS Patients*; Vanden Bossche, H., Ed.; Plenum Press: New York, 1990; pp 67–74.
- (12) Yoshida, Y.; Aoyama, Y. Yeast Cytochrome P-450 Catalyzing Lanosterol 14 $\alpha$ -Demethylation. I. Purification and Spectral Properties. *J. Biol. Chem.* **1984**, *259*, 1655–1660.
- (13) Hitchcock, C. A.; Dickinson, K.; Brown, S. B.; Evans, E. G. V.; Adams, D. J. Purification and Properties of Cytochrome P-450-Dependent 14 $\alpha$ -Sterol Demethylase from *Candida albicans*. *Biochem. J.* **1989**, *263*, 573–579.
- (14) Trzaskos, J.; Kawata, S.; Gaylor, J. L. Microsomal Enzymes of Cholesterol Biosynthesis. Purification of Lanosterol 14 $\alpha$ -Methyl Demethylase Cytochrome P-450 from Hepatic Microsomes. *J. Biol. Chem.* **1986**, *261*, 14651–14657.
- (15) Sono, H.; Sonoda, Y.; Sato, Y. Purification and Characterization of Cytochrome P-450<sub>14DM</sub> (Lanosterol 14 $\alpha$ -Demethylase) from Pig Liver Microsomes. *Biochim. Biophys. Acta* **1991**, *1078*, 388–394.
- (16) Morris, G. M.; Richards, W. G. Molecular Modelling of the Sterol C-14 Demethylase of *Saccharomyces cerevisiae*. *Biochem. Soc. Trans.* **1991**, *19*, 793–795.
- (17) Boscott, P. E.; Grant, G. H. Modeling Cytochrome P450 14 $\alpha$  Demethylase (*Candida albicans*) from P450cam. *J. Mol. Graphics* **1994**, *12*, 185–192.
- (18) Hoeltje, H. D.; Hense, M. A Molecular Modeling Study on Binding of Drugs to Calmodulin. *J. Comput.-Aided Mol. Des.* **1989**, *3*, 101–109.

- (19) Marshall, G. R.; Cramer, R. D., III. Three Dimensional Structure-Activity Relationships. *Trends Pharmacol. Sci.* **1988**, *9*, 285–289.
- (20) Massa, S.; Di Santo, R.; Artico, M.; Costi, R.; Di Filippo, C.; Simonetti, G.; Retico, A.; Artico, M. Researches on Antibacterial and Antifungal Agents. XV. 3-Aryl-4-[a-(1H-imidazol-1-yl)benzyl]-pyrroles with Potent Antifungal Activity. *Eur. Bull. Drug Res.* **1992**, *1*, 12–17.
- (21) Massa, S.; Di Santo, R.; Retico, A.; Artico, M.; Simonetti, N.; Fabrizi, G.; Lamba, D. Antifungal Agents. Synthesis and Antifungal Activities of Estrogen-Like Imidazole and Triazole Derivatives. *Eur. J. Med. Chem.* **1992**, *27*, 495–502.
- (22) Massa, S.; Di Santo, R.; Artico, M.; Costi, R.; Apuzzo, G.; Simonetti, G.; Artico, M. Novel *In Vitro* Highly Active Antifungal Agents with Pyrrole and Imidazole Moieties. *Med. Chem. Res.* **1992**, *2*, 148–153.
- (23) Massa, S.; Di Santo, R.; Costi, R.; Simonetti, G.; Retico, A.; Apuzzo, G.; Artico, M. Antifungal Agents. III. Naphthyl and Thienyl Derivatives of 1H-Imidazol-1-yl-4-phenyl-1H-pyrrol-3-ylmethane. *Farmaco* **1993**, *48*, 725–736.
- (24) Artico, M.; Massa, S.; Di Santo, R.; Costi, A.; Retico, A.; Apuzzo, G.; Simonetti, N. Antifungal Agents. 5. Chloro and Amino Derivatives of 1,2-Diaryl-1-(1H-imidazol-1-yl)ethane with Potent Antifungal Activity. *Eur. J. Med. Chem.* **1993**, *28*, 715–720.
- (25) Di Santo, R.; Massa, S.; Costi, R.; Simonetti, G.; Retico, A.; Apuzzo, G.; Troccoli, F. Antifungal Agents. VIII. Synthesis and Antifungal Activities of Bipyrryl Analogues of Bifonazole. *Farmaco* **1994**, *49*, 229–236.
- (26) Polak, A.; Hartman, P. G. Antifungal Chemotherapy - Are We Winning? *In Progress in Drug Research*, V. 37; Jucker, E., Ed.; Birkhäuser Verlag: Basel, 1991; pp 181–269.
- (27) Fromtling, R. A. Imidazoles as Medically Important Antifungal Agents: an Overview. *Drugs Today* **1984**, *20*, 325–349.
- (28) Cramer, R. D., III; Patterson, D.; Bunce, J. Comparative Molecular Field Analysis (CoMFA). 1. Effect of Shape in Binding of Steroids to Carrier Proteins. *J. Am. Chem. Soc.* **1988**, *110*, 5959–5967.
- (29) Marchington, A. F. The Design of Triazole Fungicides. *ACS Symp. Ser.* **1984**, *25*, 173–183.
- (30) Furet, P.; Batzl, A.; Bhatnagar, E.; Francotte, E.; Rihs, G.; Lang, M. Aromatase Inhibitors: Synthesis, Biological Activity and Binding Mode of Azole-Type Compounds. *J. Med. Chem.* **1993**, *36*, 1393–1400.
- (31) Greco, G.; Novellino, E.; Fiorini, I.; Nacci, V.; Campiani, G.; Ciani, S. M.; Garofalo, A.; Bernasconi, P.; Mennini, T. A Comparative Molecular Field Analysis Model for  $\epsilon$ -Arylpyrrolo-[2,1-d][1,5]benzothiazepines Binding Selectively to the Mitochondrial Benzodiazepine Receptor. *J. Med. Chem.* **1994**, *37*, 4100–4108.
- (32) DePriest, S. A.; Mayer, D.; Naylor, C. B.; Marshall, G. R. 3D-QSAR of Angiotensin-Converting and Thermolysin Inhibitors: a Comparison of CoMFA Models Based on Deduced and Experimentally Determined Active Site Geometries. *J. Am. Chem. Soc.* **1993**, *115*, 5372–5384.
- (33) Marshall, G. R. Computer-Aided Drug Design. In *Computer-Aided Molecular Design*; Richards, G. R., Ed.; IBC Technical Services Ltd.: London, 1989; pp 91–104.
- (34) PCMODEL Molecular Modeling Software, available from Serena Software, Box 3076, Bloomington, IN 47402-3076.
- (35) Gajewski, J. J.; Gilbert, K. E.; McKelvey, J. MMX an Enhanced Version of MM2. In *Advances in Molecular Modeling*; Liotta, D., Ed.; JAI Press Inc.: Greenwich, London, 1990; Vol. 2, pp 65–92.
- (36) The program BKM is available from Professor Kosta Steliou, Boston University, Boston, MA.
- (37) Botta, B.; Di Giovanni, M. C.; Delle Monache, G.; De Rosa, M. C.; Gacs-Baitz, E.; Botta, M.; Corelli, F.; Tafi, A.; Santini, A.; Benedetti, E.; Pedone, C.; Misiti, D. A Novel Route to Calix[4]arenes. 2. Solution- and Solid-State Structural Analyses and Molecular Modeling Studies. *J. Org. Chem.* **1994**, *59*, 1532–1541 and references cited therein.
- (38) The program MOPAC (Molecular Orbital Package) 5.0 is available from QCPE Creative Arts, Bldg. 181, Indiana University, Bloomington, IN, No. 455.
- (39) Sybyl (version 6.0) Molecular Modeling System, available from Tripos Associates Inc., 1699 S. Hanley Rd., St. Louis, MO 63144.
- (40) Stahle, L.; Wold, S. Partial Least Squares Analysis with Cross-Validation for the Two-Class Problem: a Monte Carlo Study. *J. Chemom.* **1987**, *1*, 185–196.
- (41) Cramer, R. D., III; Bunce, G. D.; Patterson, D. E.; Frank, I. E. Crossvalidation, Bootstrapping, and Partial Least Squares Compared with Multiple Regression in Conventional QSAR Studies. *Quant. Struct.-Act. Relat.* **1988**, *7*, 18–25.
- (42) Oprea, T.; Waller, C. L.; Marshall, G. R. Three-Dimensional Quantitative Structure-Activity Relationship of Human Immunodeficiency Virus (I) Protease Inhibitors. 2. Predictive Power Using Limited Exploration of Alternate Binding Modes. *J. Med. Chem.* **1994**, *37*, 2206–2215.
- (43) Tafi, A.; *et al.* Unpublished results. Coordination of bifonazole to protoporphyrin was studied by modification the PCMODEL MMX force field, where the imidazole ring of bifonazole is bound perpendicularly to the heme group and *gauche* to one of the iron–nitrogen bonds in the porphyrin plane. The bond distance between the iron atom and the imidazole coordinating nitrogen N3, shown in Figures 1 and 2, is 2.00 Å. All the other bond distances and bond angles agree reasonably well with experimental structural data on heme enzymes reported up to date (see: Dawson, J. H.; Sono, M. Cytochrome P-450 and Chloroperoxidase: Thiolate-Ligated Heme Enzymes. Spectroscopic Determination of Their Active Site Structures and Mechanistic Implications of Thiolate Ligation. *Chem. Rev.* **1987**, *87*, 1255–1276).
- (44) An effort was done to improve the statistical significance of the analysis performed on the 40 training set compounds aligned according to method II. The less active and worstly fitted compound (**4i**), which showed a value of  $-\log(\text{MIC}_{90}(\text{compd})/\text{MIC}_{90}(\text{bifonazole})) = -2.40$  log units and a cross-validated residual of 1.55 log units, was discarded. The new 39-compound training set gave very good cross-validated and conventional results (six components,  $r^2_{\text{cv}} = 0.72$ , SEP = 0.47 log unit,  $r^2 = 0.96$ , SEE = 0.19 log unit, F = 116.7), but the predictive ability of its “best correlation” model was poorer than the other models, showing a predictive  $r^2$  of 0.53 log unit. Due to this result, this approach was not considered further.

JM950385+